

Ahmet Gultekin Avci
Baris Barlas



<http://dx.doi.org/10.21278/brod74303>

ISSN 0007-215X
eISSN 1845-5859

Investigation of the optimum longitudinal single transverse step location for a high-speed craft

UDC 629.5.015.2:629.5.018.71:629.52

Original scientific paper

Summary

One of the crucial aspects of the conceptual design of a stepped planing hull is the prediction of its performance. To improve performance, the prediction of total resistance must become more accurate. In the field of research, both towing tank experiments and numerical analysis may be used to achieve this goal. In this study, experiments were conducted initially to investigate total resistance of a relatively high-speed craft without a transverse step. Later, numerical computations were carried out to validate the experimental results. After it was determined that the test results and CFD methods were in good agreement, the experimental method continued to investigate the resistance properties of the hull with four different configurations to evaluate the optimal longitudinal position of a single transverse step. The ideal longitudinal position of the single transverse step was evaluated based on a similar relatively high-speed hull with a velocity of up to beam Froude number (Fr_B) 2.56 in this study, focusing on the Fr_B range between 2.30 and 2.45.

Key words: planing hull; resistance; stepped hull; transverse step; CFD

1. Introduction

Although there have been numerous studies on the hydrodynamic characteristics of high-speed boats, there is still an urgent need to investigate the design of efficient planing hulls. The hull is subjected to dynamic effects such as forces and moments resulting from heave and pitch motions, which are known as trim and sinkage. Moreover, due to the rigid body's dynamic conditions, the total resistance increases rapidly at high speeds, leading to excessive fuel consumption. Typically, a high-speed ship reaches the semi-planing mode before the transient phase (which refers to the transition from the semi-planing mode to the fully planing mode) at beam Froude numbers (Fr_B) between 0.75 and 1.12. Compared to other semi-displacement hulls, the overall drag of the hull increases, albeit at a slower rate, after the transient regime. The wave resistance increases as the vessel advances through higher velocities. Therefore, all attitudes must be taken into account, along with the drag values, and accurately predicted to determine the overall resistance of the full-scale ship. [1,2].

The fluid flow and resulting hydrodynamic pressure generate hydrodynamic lift, which improves vessel operation by reducing wave making resistance and consequently, the overall resistance, allowing the vessel to reach very high speeds. A high-speed boat's resistance characteristics are predicted using model testing, however, heave and pitch motions should also be accurately assessed to be considered in ship scale evaluations. The application of steps to high-speed marine vessels has been used for many years to increase efficiency and achieve higher speeds. Steps may increase the vessel's lift coefficient since more than one maximum pressure area may emerge on the vessel's body. Air intakes through the bottom of the hull surface between the step and the front hull can also lead to a reduction in drag. Depending on their special design, high-speed boats typically may have one or more transverse steps. Furthermore, a brief literature review provides the following statements in this regard.

A method for estimating the effectiveness of stepped hulls has been developed based on the approach from "Savitsky's technique" for planing boats. The method's fundamental element is the description of the pattern of the water surface aft of the step [3]. Garland and Maki [4] suggested that selecting the greatest step possible, with the height at which the flow no longer reattaches to the afterbody serving as the upper bound for this dimension. Lee [5] showed that, the reduction in wetted surface area and friction drag are the main contributors to this decrease in resistance. Lotfi et al. [6] indicated that, when using single-step planing hulls, the total trim degree is reduced by accelerating the hull and moving the step longitudinally farther from the transom. The wetted surface area is divided into multiple smaller areas by the hull's steps. As a consequence of this, the hull will be able to plane on two or more high-aspect planing surfaces [7]. De Marco [8] declared that when simulating stepped hulls, the overset mesh technique can be used to detect total resistance and hull running attitude with a satisfactory level of accuracy. Ghadimi and Panahi [9] focus on the constant motion of yawed planing hulls, with attention to how fitting steps to the bottom of these boats affects the hydrodynamic forces and moments operating on the hull. The authors claim that the yawing moment of the studied stepped and non-stepped high-speed hulls do not differ significantly from one another. The transverse step has a positive effect on the reduction of resistance and increasing the longitudinal stability of the considered planing boats [10]. It was found that the hull's wetted area and trim angle converged with an increase in the hull's beam Froude number [11]. Esfandiari et al. [12] provided numerical simulations of the dynamics of a 2-stepped and non-stepped planing hull in an upright position when encountering head waves, addressing the problem dynamic behavior. Najafi et al. [13] mentioned the collected experimental data and stated that the overall resistance of the speed craft without a step increases as the deadrise angle increases. Furthermore, higher hull speeds and lower deadrise angles result in a lower wetted area in a non-stepped hull. Also, the stable area of the ship, which is free from porpoising, is directly related to the trim of the ship [14]. In the study [15], a mathematical model was developed and figured out that, it is possible to simulate the nonlinear motion of a double-stepped boat in waves. The study concluded that a higher front step can boost vertical acceleration while reducing heave and pitch responses. When operating at high speeds, swept aft steps provide superior dynamic stability than other step designs without decreasing resistance compared to unswept steps [16]. Besides, depending on the outcomes of the experiments of Ghadimi et al. [17], the inclusion of the transverse step improved the vessel's stability and reduced its trim. Nowruzi [18] demonstrated that decreasing the deadrise angle lowers the overall resistance, overall trim angle, and overall wetted surface of hulls without steps. Yang et al. [19], mentioned that because the step's drag reduction effect is dependent on the cavity pattern, it is vital to investigate the flow details and the relationship between pattern and hydrodynamic parameters. Najafi et al. [20], studied two-stepped hulls and stated that the longitudinal position of the aft step from the transom has an irregular effect on total resistance. Although there have been several studies on the

performance of stepped hulls in calm waters, it is important to note that the effects of step height and location, step number, and step shape are still unknown [21].

This study aims to help fill the gaps in the literature, in addition to the very few studies such as [21], by finding the optimal longitudinal location of one transverse step for an 18 m high-speed personnel boat in limited range of beam Froude numbers, which is a novelty in the related field of research on the stepped hulls. Due to the dimensions of the towing tank, the model length, high speeds, and dynamic motions of the chosen planing hull, it was necessary to validate the experiments using CFD methods, despite the reported uncertainties in the tests [22]. Thus, the model with no-step was initially investigated both experimentally and numerically. Later, the assessment of the dynamic wetted areas at $Fr_B = 2.56$ with different step configurations could be evaluated numerically, which was the second reason for performing CFD analysis. Once the good agreement between the test results and CFD methods was observed, the experimental method was used to investigate the resistance properties of the stepped hull. Within this investigation, four different step locations were considered, and a parametric study was performed with the ratio of " s/LCB " in which " s " is the longitudinal starting point of the step from the stern of the hull.

The paper is structured as follows: Section 2 presents the mathematical formulation, boundary conditions, and grid generation of the numerical domain. A rigid mesh method was employed for the hull without step, and an overset mesh method was implemented for the stepped configurations of the hull. In Section 3, the numerical method was introduced. Section 4 presents the experimental procedures both for stepped and non-stepped hull configurations. The results are presented in Section 5, including graphics. Finally, Section 6 concludes the paper with remarks on future work.

2. Mathematical formulation

2.1 Governing equations

Trim and sinkage data were modelled in the current investigation using a two-degree-of-freedom model of rigid body movement with dynamic fluid body interaction (DFBI), which replicated the motions observed in the model tests. The formula for interpreting the model body's centre of mass, which is used to estimate trim and sinkage values, is provided below:

$$M \frac{\partial}{\partial t} \omega = n \quad (1)$$

and

$$m \frac{dv}{dt} = f \quad (2)$$

In the provided formula, f represents the total force and n represents the total moment acting on the solid body in accordance with M , which denotes the inertial moment with regard to the rotating axis, ω is the rigid body's angular velocity relative to the axis of rotation, and m is the model's mass. The resultant force impacting on the hull surface is denoted by f , while the speed of LCG is denoted by v . Fluid pressure and shear force acting on each body boundary face were used to calculate the force and moment acting on the model as a result. The model's translations were computed using the flow domain's predicted velocity and pressure fields [22]. It is also mentioned in [23] that, the unsteady RANS equations for an incompressible, 3-D flow are the continuity equation:

$$\frac{\partial U_i}{\partial x_i} = 0 \quad (3)$$

and the momentum equation:

$$\frac{\partial U_i}{\partial t} + \frac{\partial(U_i U_j)}{\partial x_j} = -\frac{1}{\rho} \frac{\partial P}{\partial x_i} + \frac{\partial}{\partial x_j} \left[\nu \left(\frac{\partial U_i}{\partial x_j} + \frac{\partial U_j}{\partial x_i} \right) \right] - \frac{\overline{\partial u_i' u_j'}}{\partial x_j} \quad (4)$$

Here, x_i is the spatial coordinate, t is period of time, U_i is the mean velocity, u_i' is the varying velocity, P is the average pressure, ρ is the fluid density and ν is the kinematic viscosity. The Boussinesq approximation models the Reynolds stress tensor:

$$\overline{u_i' u_j'} = -\nu_t \left(\frac{\partial U_i}{\partial x_j} + \frac{\partial U_j}{\partial x_i} \right) + \frac{2}{3} \delta_{ij} k \quad (5)$$

The eddy viscosity was evaluated using the conventional k - ε turbulence closure model. The eddy viscosity, ν_t , can be expressed as $\nu_t = C_\mu k^2/\varepsilon$, where C_μ is a constant assumed to be 0.09, k is the turbulent kinetic energy and ε is the dissipation rate of k . The standard k - ε turbulence model was used to derive the turbulence quantities, k and ε , using a set of transport equations. The equations for turbulent kinetic energy, k , and the rate at which the turbulent energy is dissipated, ε , can be given as;

$$\frac{\partial k}{\partial t} + \frac{\partial(k U_j)}{\partial x_j} = \frac{\partial}{\partial x_j} \left[\left(\nu + \frac{\nu_t}{\sigma_k} \right) \frac{\partial k}{\partial x_j} \right] + P_k - \varepsilon \quad (6)$$

$$\frac{\partial \varepsilon}{\partial t} + \frac{\partial(\varepsilon U_j)}{\partial x_j} = \frac{\partial}{\partial x_j} \left[\left(\nu + \frac{\nu_t}{\sigma_\varepsilon} \right) \frac{\partial \varepsilon}{\partial x_j} \right] + C_{\varepsilon 1} P_k \frac{\varepsilon}{k} - C_{\varepsilon 2} \frac{\varepsilon^2}{k} \quad (7)$$

$$P_k = -\overline{u_i' u_j'} \frac{\partial U_i}{\partial x_j} \quad (8)$$

where, $C_{\varepsilon 1}=1.44$, $C_{\varepsilon 2}=1.92$ and the turbulent Prandtl numbers for k and ε are $\sigma_k = 1.0$, and $\sigma_\varepsilon = 1.3$. The semi-implicit technique, (SIMPLE) algorithm, for pressure-linked formula, is used to address the pressure and velocity coupling problem, where a putative pressure is utilized to solve the velocity field first. The computed pressure and velocity values are then employed to adjust the pressure and velocity fields, as reported in the study [24]. For one half of the model hull, calculations are performed within an unstructured finite volume mesh that is symmetric along the axial centreline.

The phase distributions and the position of the interfaces are defined by the volume fraction. This term is expressed as follows:

$$\alpha_i = \frac{V_i}{V} \quad (9)$$

where, V_i is the volume of phase i in the cell and V is the volume of the cell. Besides, sum of the volume fractions of all phases must be equal to one. Also, phase i is distributed by the mass conservation equation as:

$$\frac{\partial}{\partial t} \int_V \alpha_i dV + \oint_A \alpha_i v \cdot da = \int_V (S_{\alpha_i} - \frac{\alpha_i}{\rho_i} \frac{D\rho_i}{Dt}) dV - \int_V \frac{1}{\rho_i} \nabla \cdot (\alpha_i \rho_i v_{d,i}) dV \quad (10)$$

where, a is the surface area vector, v is the mass-averaged mixture velocity, $v_{d,i}$ is diffusion velocity, S_{α_i} is user-defined source term of phase i and $D\rho_i/Dt$ is Lagrangian or material derivative of the phase densities ρ_i .

2.2 Numerical Study, Boundary Conditions and Grid Generation.

To minimize the computational cost, a half-model methodology was employed, resulting in a symmetry plane that splits the domain along the centreline. Fig. 1 shows the virtual towing tank domain together with the model geometry and boundary conditions. The domain covered double hull lengths in front of the model, three lengths behind, double hull lengths through the beam considering wave diffraction, and three lengths in negative z direction (depth). To eliminate interaction between true and reflected waves, a wave damping length of $1L$ was used. The domain was partitioned using 4,557,600 grid points for the numerical simulations, with the rigid mesh localized adjacent to the hull and free surface. To properly manage the complex mesh generation, a trimmed cell mesher was used. As shown in Fig. 2, the finite volume mesh was constructed utterly in [25] comprising structured hexahedral grids, and the mesh assessment is given in Table 1. Walls with slip boundary conditions were employed in the far field.

In the case of free slipping, the wall shear stress is zero. Thus, the walls at the model surface were specified with a no-slip circumstance implying a velocity gradient parallel to the wall that is zero. At the tank outlet boundary, a derivative of zero condition in the axial direction was used, and the pressure was hydrostatic. At the boundaries of the symmetry plane, a zero-derivative criterion in the normal directions was applied.

The well-behaved structure and reliable computations deemed the conventional $k-\varepsilon$ turbulence model the preferred approach. Further wall routines are required to integrate solution parameters between the wall and the fully turbulent zone when applying the standard $k-\varepsilon$ two-equation turbulence model. The velocity varies logarithmically in the log-law zone with the average wall distance y^+ as illustrated in equation (11) below. Despite minor variations in the literature, according to Stanford standards, quantities of universal factors, the Von Karman constant, $\kappa = 0.41$ and the constant $B = 5.0$, as stated by Dixit and Ramesh [26].

$$U^+ = \frac{1}{\kappa} \ln(y^+) + B \quad (11)$$

Where, U^+ is the streamwise velocity non-dimensionalized by the friction velocity u_τ . After the solution has converged, the distribution of the standardized wall distance (y^+) throughout the model surface at $Fr_B=2.34$ is depicted in Fig. 3. The wall function deployment, where it is projected that the y^+ values would exceed 30, it is consistent with the y^+ values on the hull, which were estimated to range from 45 to 60.

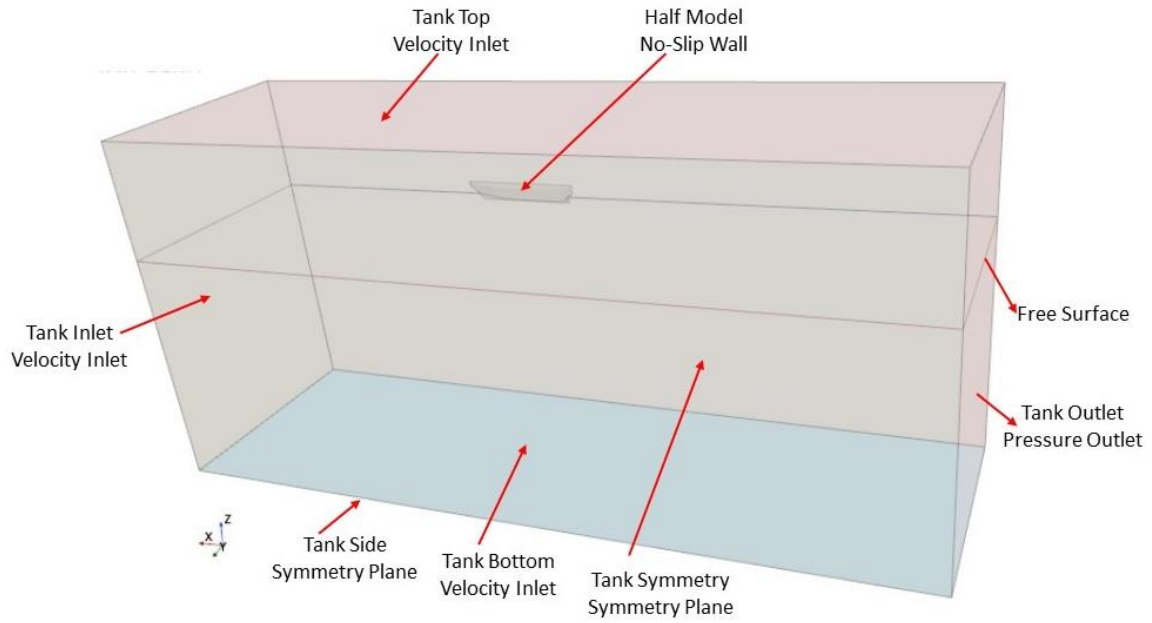


Fig. 1 Computational Domain of Numerical Towing Tank.

Table 1 Grid evaluation (rigid mesh)

Zone	Zone Name	Cell Sizes
1	Field Far	0.145 L
2	Mid domain-1	0.090 L
3	Mid domain-2	0.073 L
4	Free surface & Near model surface	0.005 L
5	Model & Free surface	0.037 L

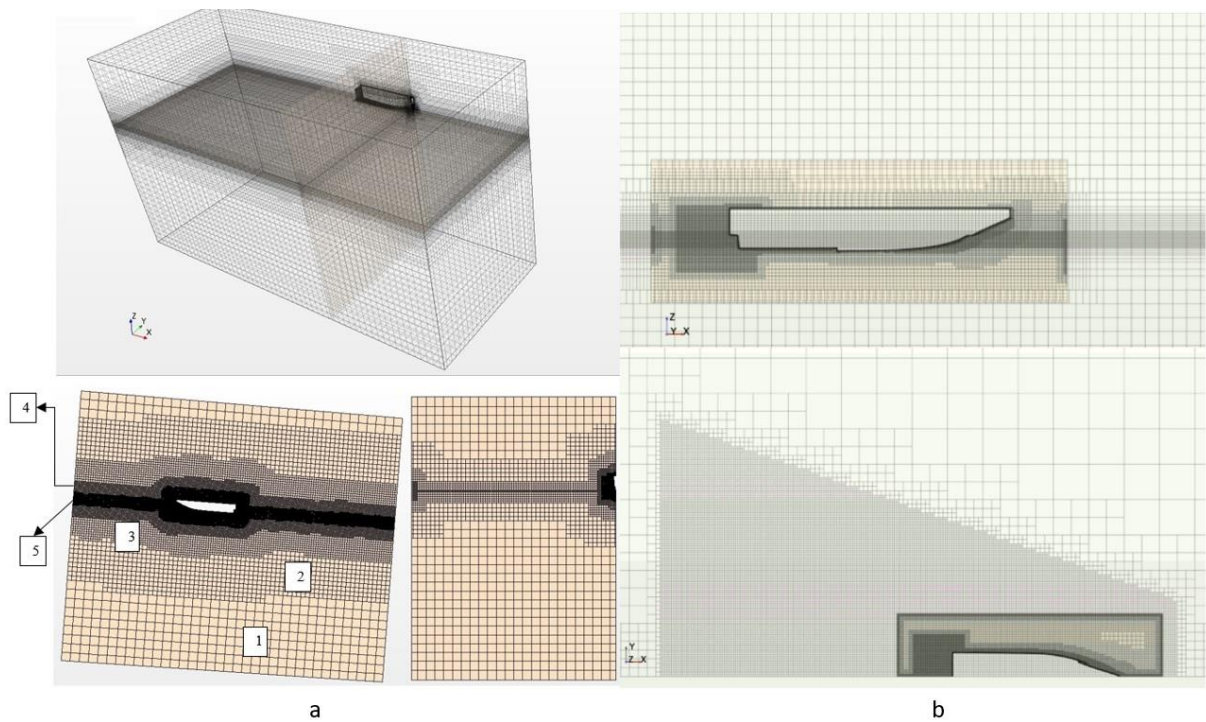


Fig. 2 Hull geometry and the grids of the domain a) rigid mesh with no step b) overset mesh with step.

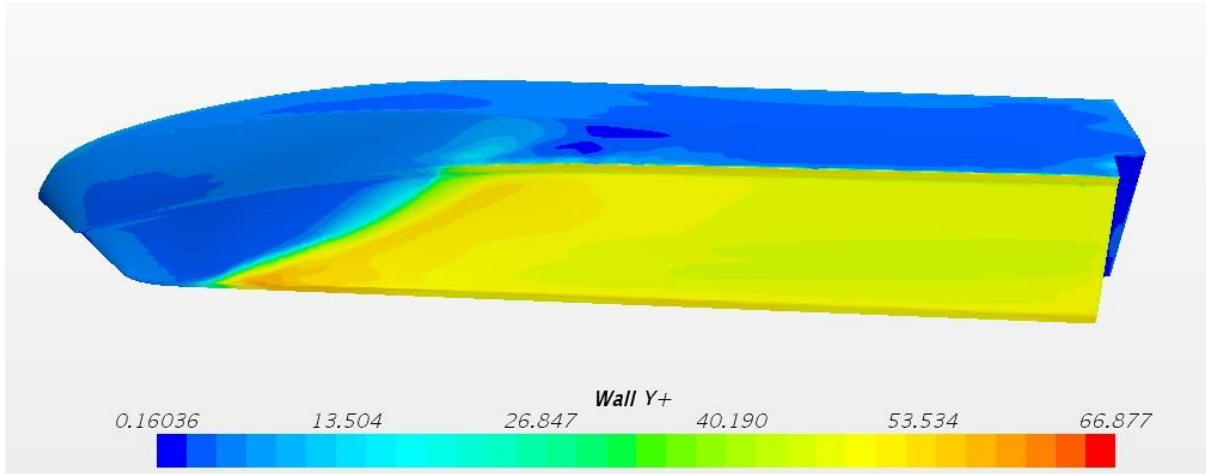


Fig. 3 y^+ distribution around the model surface at $Fr_B=2.34$.

3. Numerical method

Within this article, numerical computations of a high speed boat were carried via the RANS-based CFD software Siemens PLM Star-CCM+, which supports 3-D volume of fluid (VOF) model simulations to mimic the free surface between air and water. To generate the Eulerian Multiphase model, which matched the average temperature of the fresh water towing tank, air and water components with fixed density and dynamic viscosity were employed. A node-based finite volume algorithm was implemented to discretize the governing equations. An interpolation method of first-order upwind scheme was used to discretize the advection terms. Following each other, the governing equations were resolved. A three-stage numerical method was used: the velocity factors, the pressure and then the intensities of turbulence were assessed. In addition, the topological domain is discretized using the finite volume approach. Eulerian multiphase cases were modelled using the Multiphase Segregated Flow (MSF) model. According to [18], the term “segregated” alludes to the solution procedure’s usage of the well-known SIMPLE algorithm, which separates the pressure and velocity solvers to control the comprehensive solution. For every Eulerian phase involved in the simulation, the MSF model resolves a set of conservation equations. It is better suited for flows with a uniform density. The volume fraction represents the portion of the flow domain occupied by each component, and each of them has its own physical features. The implicit unsteady solver was employed to manage the calculations at physical time-steps. To converge the solution for each physical time-step, inner iterations are used in the implicit unsteady method. Internal iterations can be carried out by using spatial integration schemes [27].

Additionally, the VOF model was employed to imitate the waves resulting from the interaction of surface gravity with water and air. It can create flat, first and fifth order waves for a wide range of applications. For this investigation, a planar wave formation was applied to simulate the free surface of calm water. The CFL number, which connects the size of the cell to the flow rate and time step, should not exceed or be equal to one in order to maintain numerical stability [28]. According to the ITTC’s suggested procedures, the time-step for the current investigation was chosen to be between $0.005-0.01L/U$ (where L is the length of the waterline and U is velocity) [29].

Due to the hull’s rotating body motion, some amount of air espouses beneath the hull, resulting in the stated challenge regarding numerical ventilation. Due to high trim values, the volume of air flowing beneath the hull increases as the hull speed increases. Air may be observed under the hull despite the application of an overset mesh approach or various

alternative mesh refining techniques. It was noted that mesh advancements do not alleviate this problem. In most cases, this issue might result in an unintended drag decrease of up to 30% [25]. In the current study, the phase replacement technique was used to address this problem, as reported by [25]. This approach replaces the water phase with the unwanted air phase in the specified locations. The same numerical method with an overset mesh technique was used for the stepped configurations at $Fr_B=2.56$.

4. Experimental procedure

Ata Nutku Ship Model Basin at Istanbul Technical University (ITU) hosted the experiments for the current investigation. The tank had the following measurements: 160 meters in length, 6 meters in breadth, and 4 meters in depth; for the testing, the water level was arranged at 3.4 m. The towing carriage has extremely accurate speed control and can accelerate up to 5 m/s. In the towing tank, a wooden model of an 18.7 m long high-speed personnel boat with a scale of 8.5 was used for the required loading conditions, as illustrated in Fig. 4.



Fig. 4 The wooden hull model.

Table 2 summarizes the geometric and hydrostatic characteristics of the model as well as those of the fast-speed personnel boat. Fig. 5 and Fig. 6 depict the sectional lines and

profile view of the hull, respectively. In addition, the experimental setup is shown in Fig. 7. Trim and sinkage model for the proposed study is illustrated in Fig. 8.

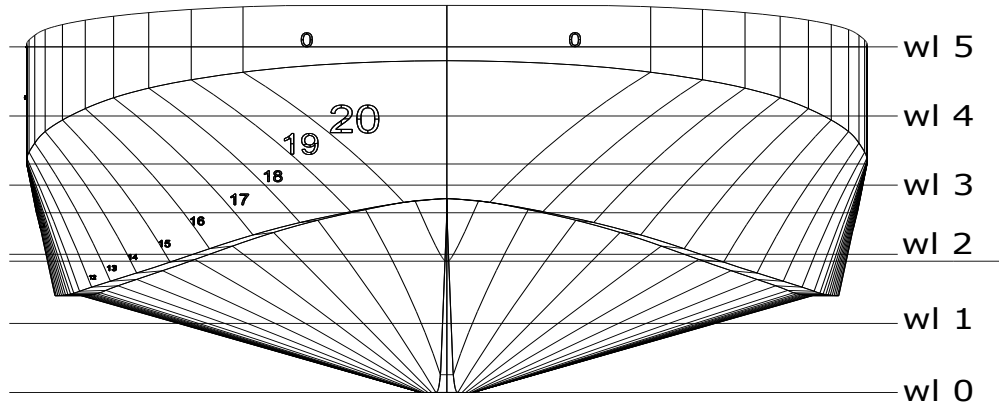


Fig. 5 Sectional curves of the model [25]

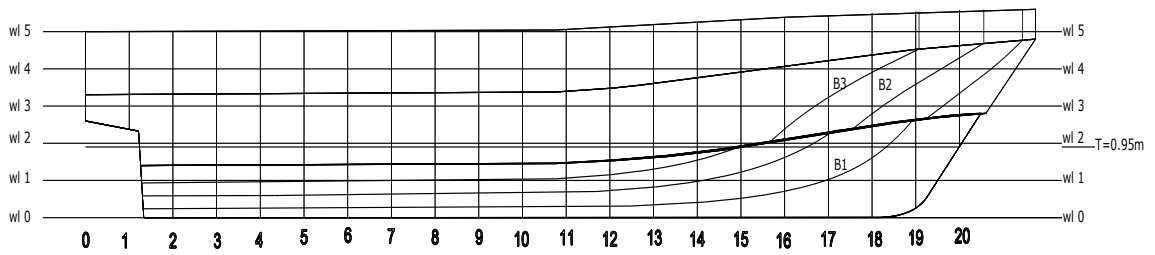


Fig. 6 View from profile of the hull [25]

Table 2 The model's and the boat's geometric and hydrostatic specifications (the hull with no-step) [25].

Main Particulars	Model ($\lambda=8.5$)	Ship
Length between perpendiculars L_{BP} (m)	2.031	17.262
Length on waterline L_{WL} (m)	1.934	16.439
Breadth B (m)	0.588	5.000
Draught (amidships) T (m)	0.111	0.950
Volume ∇ (m ³)	0.053	32.750
Displacement Δ (ton)	0.053	33.569
Nominal wetted surface area S_0 (m ²)	0.989	71.520
Block coefficient C_B	0.436	0.436
Longitudinal center of buoyancy LCB (m) (from transom)	0.833	7.080
Design speed V_S	4.77 m/s	27.0 kts

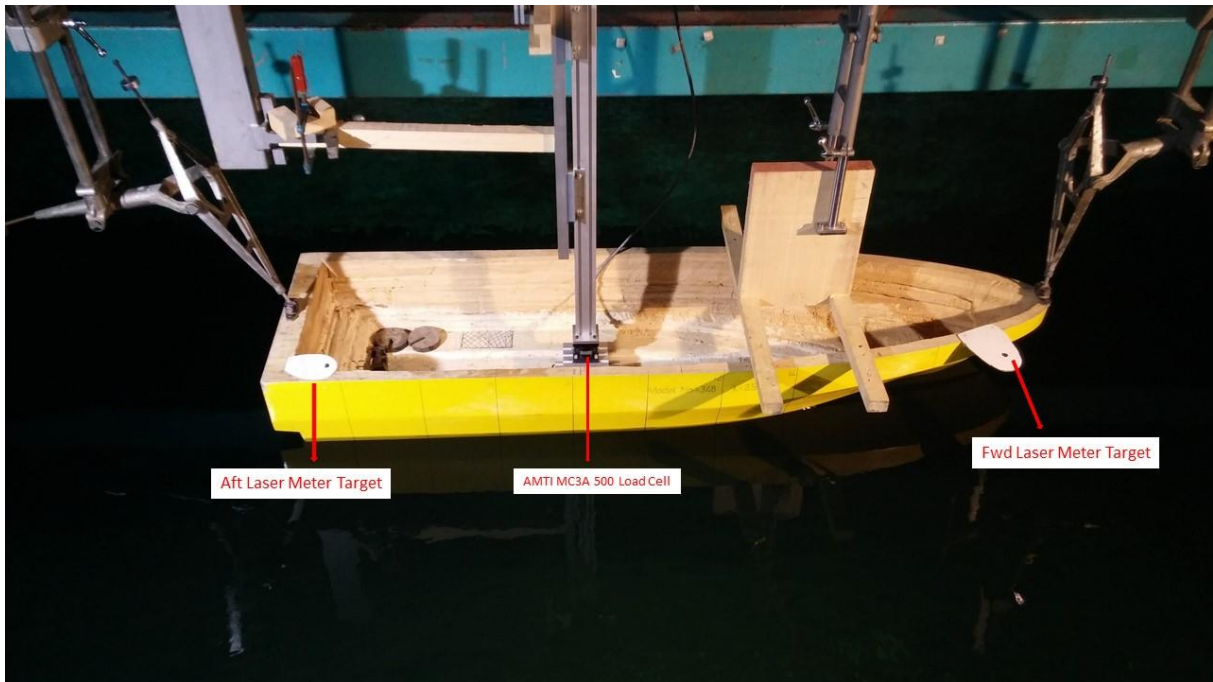


Fig. 7 Experimental setup of the towed model [25]

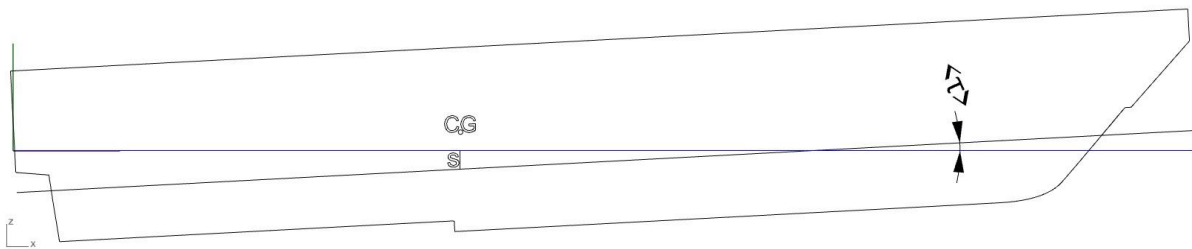


Fig. 8 Trim and Sinkage model of the system. (*s*: sinkage, *r*: trim, CG: centre of gravity)

The model was placed to the test with speeds between 10 and 34 knots on the ship scale. The tests were carried out in line with ITTC guidelines [29]. The longitudinal centre of gravity, which is corresponding to the LCB without starting trim angles, was adopted as the towing point. Besides, the model was not restrained to move in heave and pitch motions due to the experimental configuration. To explain the drag measurements, no appendages were present on the hull model as the boat was propelled by a water jet system. A load cell was utilized to measure the drag force, and a data acquisition board with a continuous sample rate of 100 Hz was used to record all of the collected data. Using the ITTC 1978 line, the drag data were scaled up to full scale, and all results were adjusted to a water temperature of 15 °C. As also mentioned in [30], several experimental methods are available for evaluating the trim and sinkage attitudes of models in the basins. During the model testing, the fore-and-aft point running sinkage measurements, which are collected by laser distance meters, were used to derive the trim angle values [25].

The hull model has been modified for the steps after the experimental and numerical outputs were validated. After the modification, the hull model was towed with different speeds and longitudinal step locations to investigate the effects of the steps on the resistance characteristics. Four different step locations were considered, and a parametric study was conducted with the ratio of “ s/LCB ”, where “ s ” is the lateral length of the step from transom of the hull. For all step locations, a fixed depth of $4\%B$ as hs/B of 20 mm was applied for step depths. Lee et al. [31] reported that the optimum step height is about $4\%B$. Different

longitudinal step locations are given in non-dimensional form in Table 3. Model hull step creation work scenes and longitudinal locations of the steps on the model hull are illustrated in Fig. 9 and Fig. 10, respectively.

During the experiments, the model is positioned upright as in the previous sections, and no appendages was during the measurements used in this part.



Fig. 9 Model hull step creation work [32]

Table 3 Longitudinal Step Locations (constant step height % (h_s/B) = 4 (20 mm))

Condition	s/LCB	s/LWL
Without Step	0.000	0.000
Step 1	0.313	0.135
Step 2	0.653	0.281
Step 3	0.976	0.420
Step 4	1.299	0.559



Fig. 10 Longitudinal locations of the steps on the model hull [29]

5. Results and discussion

This section includes information on performance prediction and ship scale comparison results for the base bare hull, as well as the effect of step locations on resistance characteristics. Fig. 11 shows the non-dimensional resistance coefficient results in Rt/Δ with respect to Fr_B , and Fig. 12 depicts the percentage deviation of the calculated R_{TM} in comparison to the experimental data. Froude numbers and ship scale velocities in tested cases are given in Table 6, while Table 7 displays the percentage errors in both drag and C_{TM} . Up to $Fr_B = 0.75$, the results of both tests and CFD, are substantially equivalent, as seen in Fig. 11 and Fig. 12. The maximum error was 2.86 % when the numerical ventilation issue was solved using the phase replacement method, indicating good agreement between the results and experimental data. Free surface wave contours generated by the model hull at $Fr_B = 2.34$ are shown in Fig. 13. Also, in Fig. 13, a typical wave pattern around a planing hull can be seen at various Froude numbers. Fig. 14 depicts the numerical approach scenes of the body and free surface elevation for various Fr_B values during the planing phase. Fig. 15 presents images from the tests without step application at different Froude numbers. From the same figure, it can be observed that the spray volume increased with the increase in the speed, as mentioned in the study [33]. Besides, corresponding to the beam Froude numbers in this study, the speed range between beam Froude numbers 0.6 and 1.5 can be considered as semi-planing mode, 1.5-2.0 range as transient regime, and starting with 2.0 and above is planing regime.

5.1 Verification Study

The Grid Convergence Index (GCI) method is employed in the verification investigation in the current study, which is based on Richardson Extrapolation. Roache [34] developed the GCI method, which has since been applied in a vast number of investigations. To evaluate the uncertainties arising from grid spacing, Celik et al. [35], utilized a detailed approach that is described in the current study. Since it is recommended by ITTC, the

refinement factor (r) is chosen as $\sqrt{2}$. The methods proposed by Celik et al. [35] can be summarized as follows:

Because the verification technique is implemented to a three-dimensional problem, the ratio of total grid cell numbers of various qualities is defined as follows.

$$r_{21} = \left(\frac{N_1}{N_2} \right)^{\frac{1}{3}} \text{ and } r_{32} = \left(\frac{N_2}{N_3} \right)^{\frac{1}{3}} \quad (12)$$

where $N1$, $N2$, and $N3$ are the total cell numbers and $N3 < N2 < N1$. The difference between the numerical scalar result of total resistance ratio between two different grid cells can be calculated as follows.

$$E_{21} = \phi_2 - \phi_1 \text{ and } E_{32} = \phi_3 - \phi_2 \quad (13)$$

The numerical solutions convergence condition can then be found by dividing the by the following Equation.

$$R = E_{21} / E_{32} \quad (14)$$

Equation below explains the ratio R 's mathematical meaning.

$-1 < R < 0$ Oscillatory convergence

$0 < R < 1$ Monotonic convergence (15)

$R < -1$ Oscillatory divergence

$1 < R$ Monotonic divergence

Subsequently, apparent order of p (order-of-accuracy) can be calculated as follows.

$$p_{RE} = \frac{\ln |E_{32} / E_{21}|}{\ln(r_{21})} \quad (16)$$

The extrapolated value also can be calculated as follows.

$$\phi_{ext}^{21} = (r^{p_{th}} \phi_1 - \phi_2) / (r^{p_{th}} - 1) \quad (17)$$

Additionally, the approximate relative error and the extrapolated relative errors are,

$$e_a^{21} = \left| \frac{\phi_1 - \phi_2}{\phi_1} \right| \text{ and } e_{ext}^{21} = \left| \frac{\phi_{ext}^{21} - \phi_1}{\phi_{ext}^{21}} \right| \quad (18)$$

Finally, the GCI index is calculated by:

$$GCI^{21} = \frac{1.25 \times e_a^{21}}{r_{21}^{p_{re}} - 1} \quad (19)$$

Three different grid schemes have been investigated at the 2.56 beam Froude number to calculate the total resistance ratio and given in Table 4. As the grid resolution increases in density, the total resistance values eventually decrease. As shown in table 5, while the convergence condition R appears to have monotonic convergence properties, it is the strongest sign of this behaviour (Table 5).

Table 4 Resistance ratios at $Fr_B = 2.56$ by different grid qualities.

Grid Quality	Rigid Mesh Method		Overset Mesh Method	
	Total Number of Cells	$Rt/\Delta (\phi_i)$	Total Number of Cells	$Rt/\Delta (\phi_i)$
Fine	8.902 x 106	0.2006	5.752 x 106	0.2056
Medium	4.558 x 106	0.2027	2.516 x 106	0.2070
Coarse	2.705 x 106	0.2084	1.148 x 106	0.2111

Besides, as specified by [36], an order of accuracy above 2.0 (the formal order of accuracy) may likely to cause too small error estimation. Maximum difference between all the solutions available (Δ_M) is 7.78×10^{-3} for rigid method and 5.54×10^{-3} for overset method. For monotonic convergence with $P_{RE} \geq 2.05$, U_ϕ is defined by Eça and Hoekstra [37] as;

$$U_\phi = \max(1.25\delta_{RE}^* + U_s, 1.25\Delta_M) \quad (20)$$

and given in Table 5 below.

Table 5 Uncertainty assessment results of numerical analysis.

	CGI Rigid Mesh	CGI Overset Mesh
r_{21}	1.25	1.32
r_{32}	1.19	1.30
R	0.370	0.338
P_{th}	2.00	2.00
P_{RE}	2.87	3.13
ϕ_1	0.2006	0.2056
ϕ_2	0.2027	0.2070
ϕ_3	0.2084	0.2111
Φ_{Ext}	0.1994	0.2049
$e_a^{21} \%$	1.00	0.70
$e_{ext}^{21} \%$	0.60	0.60
$GCI_{21} \%$	0.769	0.435
$U_{RE} \%$	0.297	0.208
$U_\phi \%$	0.972	0.692

Table 6 Froude numbers and ship scale velocities in tested cases

Fr_B	Fr	Fr_V	V_m (m/s)	V_s (knots)
0.75	0.40	0.91	1.75	9.94
0.93	0.50	1.13	2.18	12.33
1.12	0.60	1.36	2.62	14.85
1.31	0.70	1.60	3.06	17.37
1.50	0.81	1.83	3.51	19.89
1.68	0.90	2.05	3.93	22.28
1.87	1.00	2.28	4.38	24.80
2.06	1.11	2.51	4.82	27.31
2.24	1.20	2.73	5.24	29.70
2.56	1.38	3.12	5.99	33.94

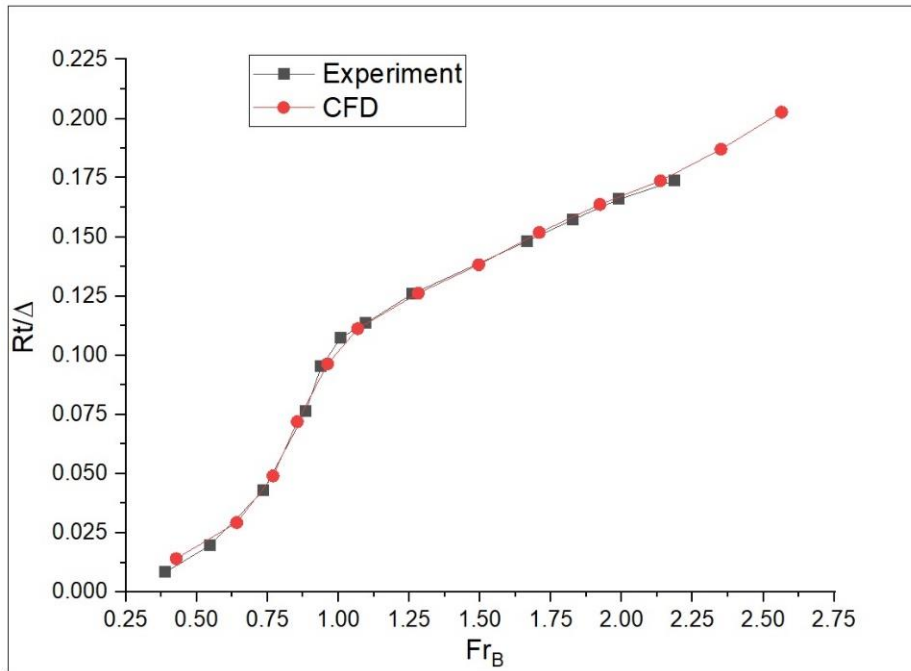


Fig. 11 Comparison of simulation results and experimental data: total resistance variation (Rt/Δ) vs Fr_B for the model size of the hull with no-step.

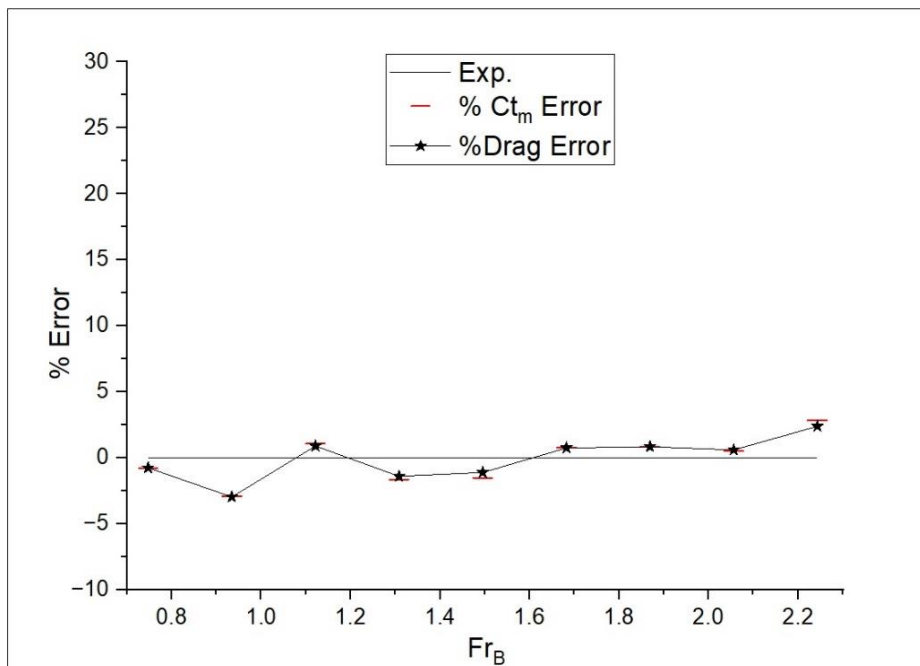
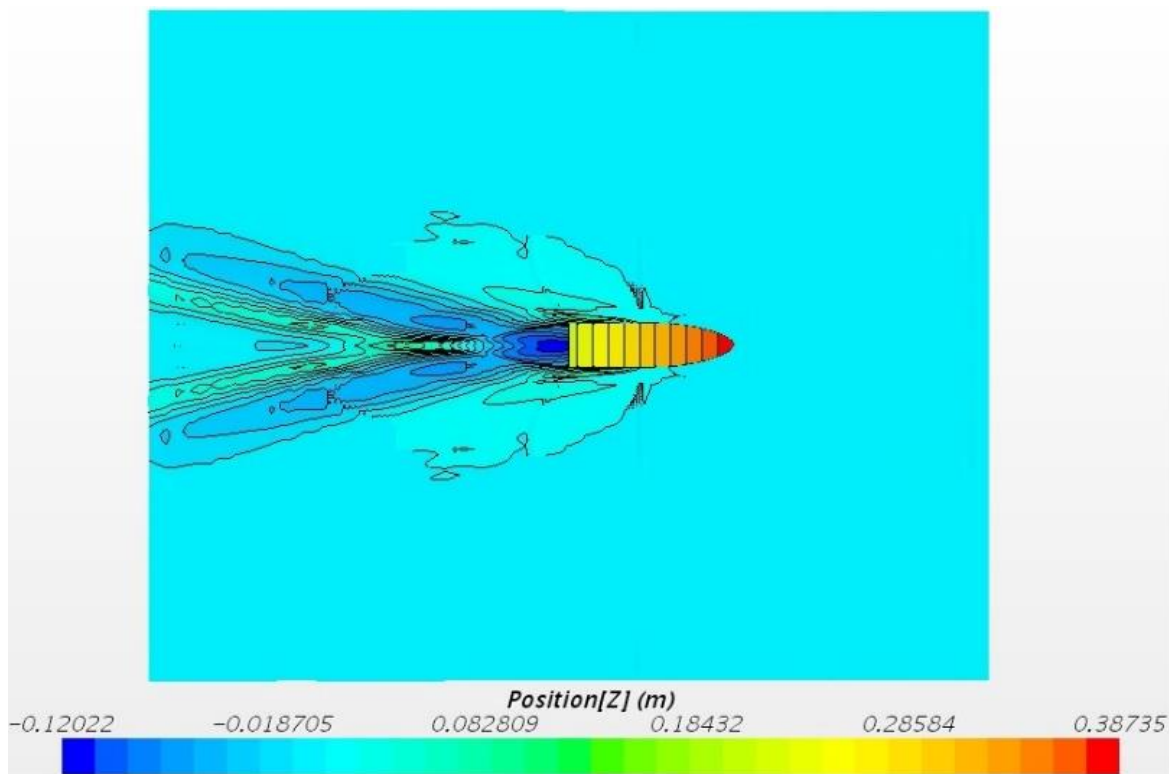


Fig. 12 Resistance errors as a percentage of the experimental data of the hull with no-step.

Delen and Bal [33] conducted an uncertainty analysis of the resistance tests using ITTC (2014) data for the same hull model as in the current research. According to the data, the extended uncertainty value for the resistance tests at $Fr_B = 1.68$ was 0.42%. Moreover, it was observed that the measurement system uncertainty sources become less effective as the hull velocity increases.

Table 7 Percentage of CFD errors vs the results of the experiment

Fr_B	% Drag error CFD vs Exp.	% C_{TM} error CFD vs Exp.
0.75	-0.75	-0.77
0.93	-2.96	-2.90
1.12	0.90	1.07
1.31	-1.40	-1.63
1.50	-1.10	-1.51
1.68	0.75	0.77
1.87	0.84	0.83
2.06	0.61	0.53
2.24	2.39	2.86

**Fig. 13** Hull wave contours at $Fr_B=2.34$

The trim and sinkage values are illustrated in Fig. 19 and Fig. 20. The sinkage values are dimensionless and expressed as sinkage/LWL.

The negative numbers in Fig. 20 indicate sinkage, while the positive numbers indicate the model rising at LCG. As a result, the model starts to rise once it enters the transient phase, or Fr_B higher than 1.10. The CFD approach and experiments are both effective in evaluating the trim and sinkage attitudes of high-speed hulls. Due to the nature of the model testing, only the overall resistance in model scale, which is made up of friction and waves, was evaluated. Empirical formulas can be used to compute the frictional resistance for both the model and the full-scale implementation. The ITTC-78 approach was utilized in the current investigation to extrapolate the drag [29]. Form factor study was disregarded because the model was designed as a high-speed hull ($k=0$). Due to the employment of the water jet propulsion system at ship scale, testing was only done on a bare hull, and the appendage coefficient was excluded. Fig.17 shows the ship scale CT_S and CF_S in respect to Fr_B , indicating that both numerical and

experimental results of total resistance coefficients are in good agreement, and the friction coefficients are nearly overlapped. Additionally, dynamic wetted surface areas and dynamic wetted lengths were used in the related calculations in non-stepped conditions, following the dynamic scaling procedure. The bottom views for the volume fraction of water scenes are illustrated in Figure 16 for the stepped hull configurations at $Fr_B=2.56$, corresponding to $Fr_V=3.12$. For the stepped configurations, the available values of dynamic-wetted areas, which were collected from the CFD analysis at $Fr_B=2.56$, corresponding to $Fr_V=3.12$, are as follows: 0.534 m^2 for step 1, 0.602 m^2 for step 2, 0.684 m^2 for step 3 and 0.669 m^2 for step 4 configurations.

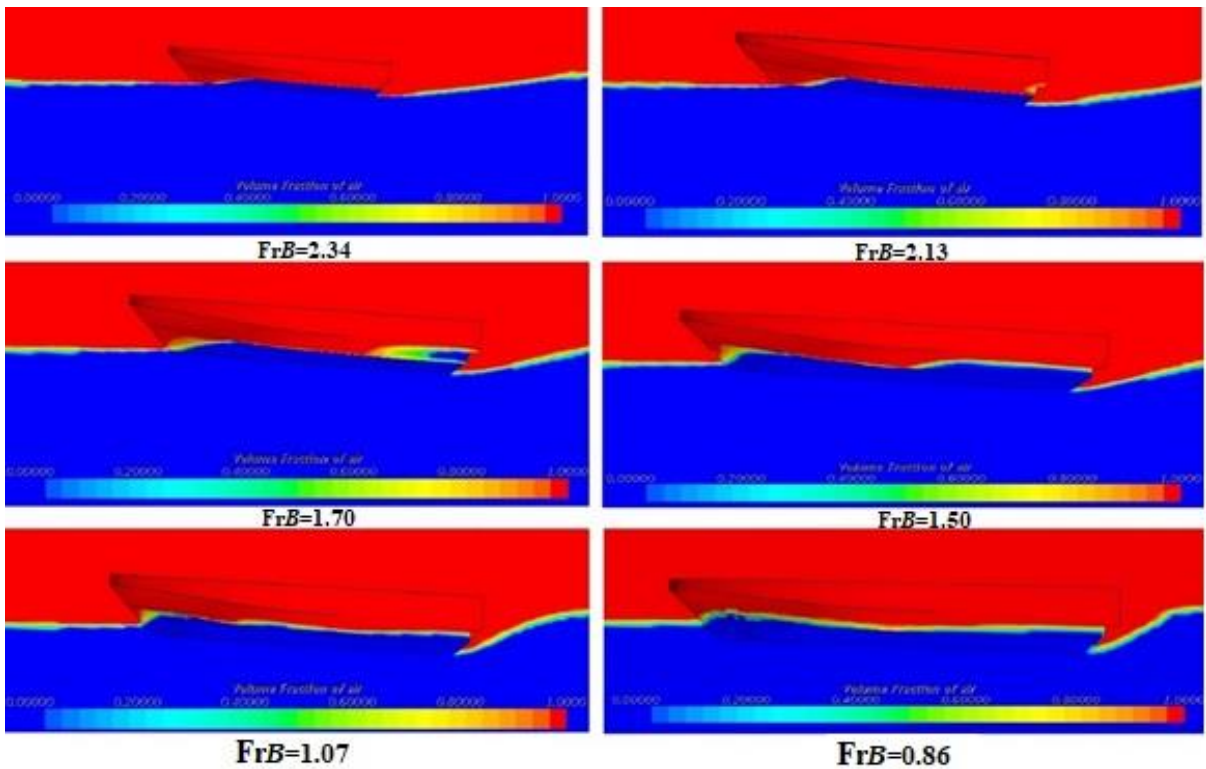


Fig. 14 At varying Fr_B values, the model hull and free surface elevations of the hull with no-step.

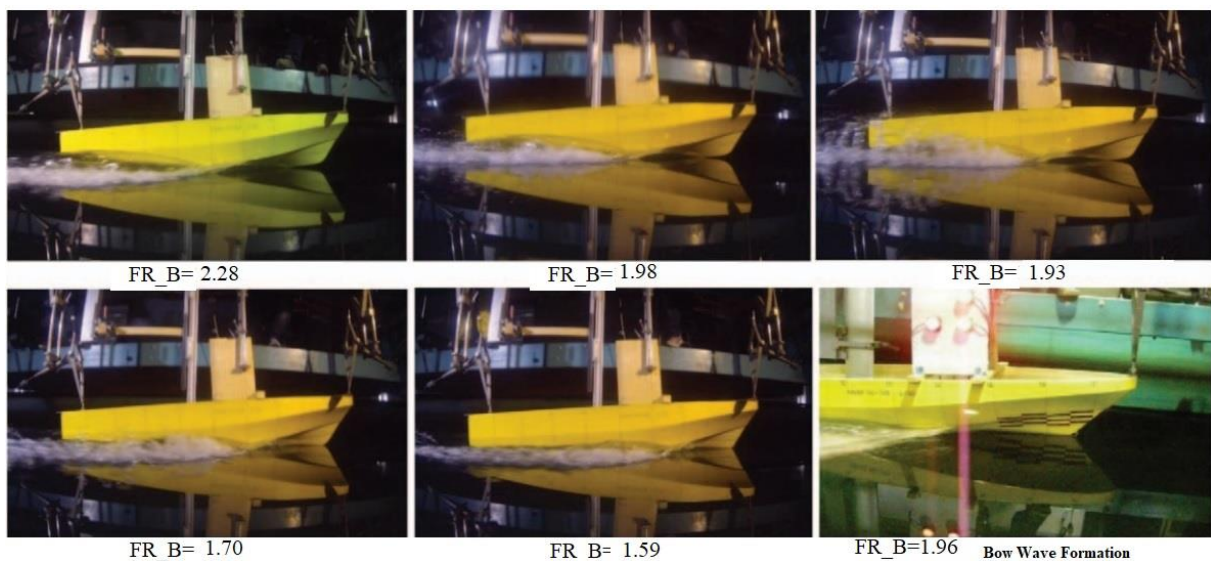


Fig. 15 During model testing, the model hull at various Fr_B values of the hull with no-step.

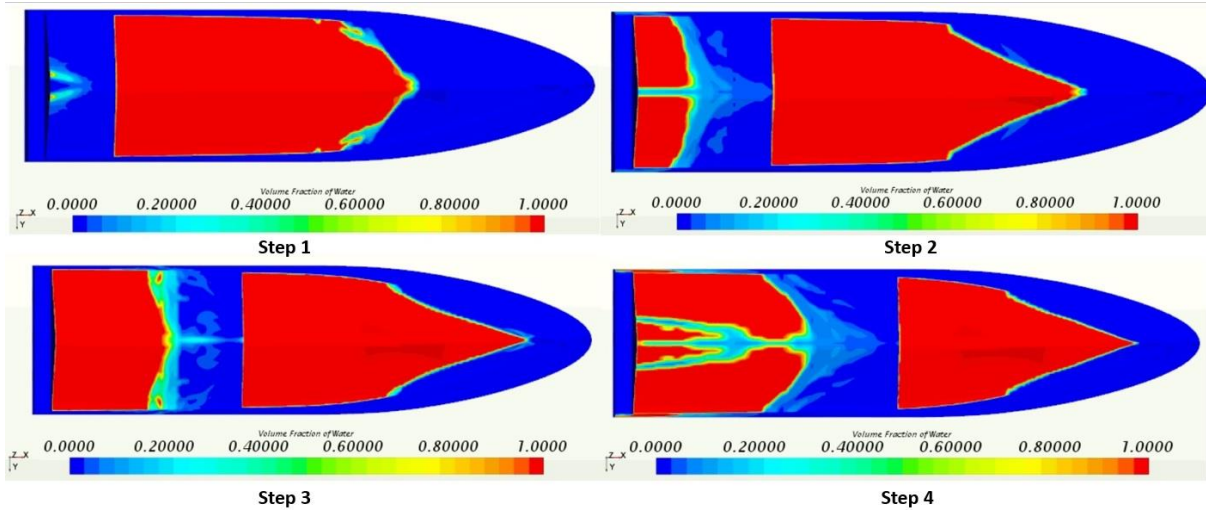


Fig. 16 Wetted areas viewed from the bottom of the hull with steps ($Fr_B=2.56$ and $Fr_V=3.12$).

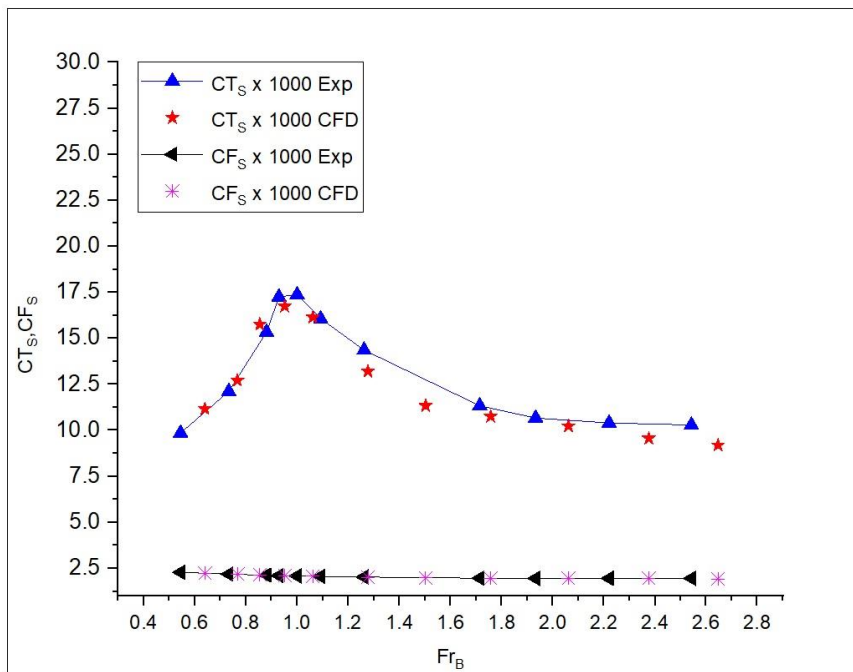


Fig. 17 Total and frictional resistance coefficients at full scale of the hull with no-step

Based on CFD estimates and experimental results obtained from sea trials, the deviations from effective power requirements were 1.7 % and 1.6 %, respectively. As a consequence, there is significant congruence between the CFD approach, experiments, and ship scale trial results for the hull without step application before the results of the optimum step location.

The variation of trim values in degrees with respect to Fr_B is given in Fig. 18 for the bare hull without steps and with different step applications. Moreover, it can be observed from Fig. 19 that the trim values start to decrease after $Fr_B=2.15$ for all cases. Furthermore, the rate of decrease in trim values is observed to increase when the s/LCB ratio shifts in the $+x$ direction. The case with step 4 shows the minimum trim value, while the case without step has the maximum trim value. As mentioned before in the introduction section, steps may increase the vessel's lift coefficient since more than one maximum pressure area may emerge on the vessel's body. For the step 4 configuration at high speeds, the pressure area is much more than the other configurations hence step 4 configuration affects the trim angle more

remarkably. This shows that step application can decrease the undesirable trim values and potentially reduce the total resistance, as demonstrated in the following plots. Because of the dynamic motions of the hull, not only trim values but also sinkage and raise of the hull rates vary and are depicted in Fig. 19.

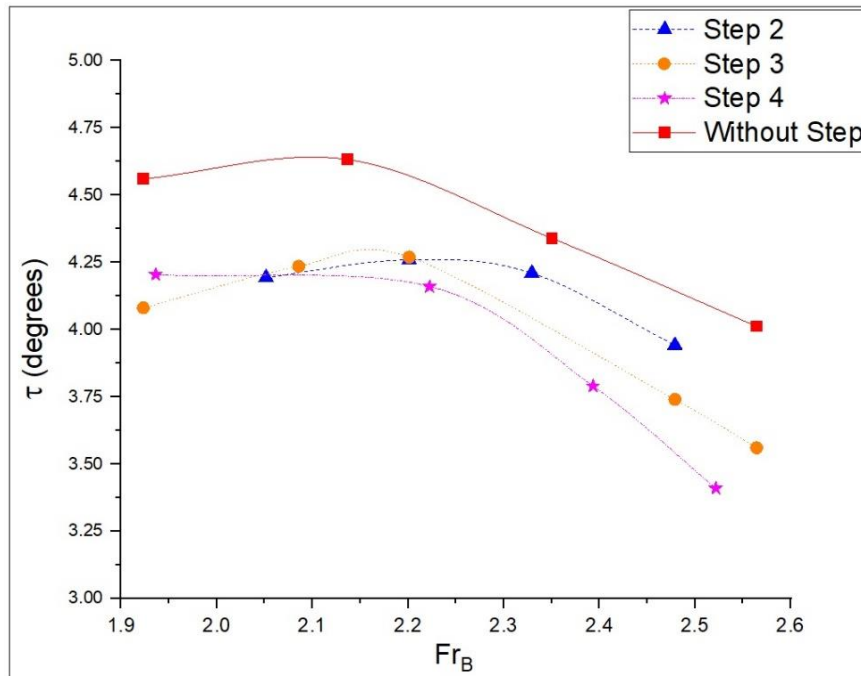


Fig. 18 Comparison of the trim in degrees for different step locations and without step.

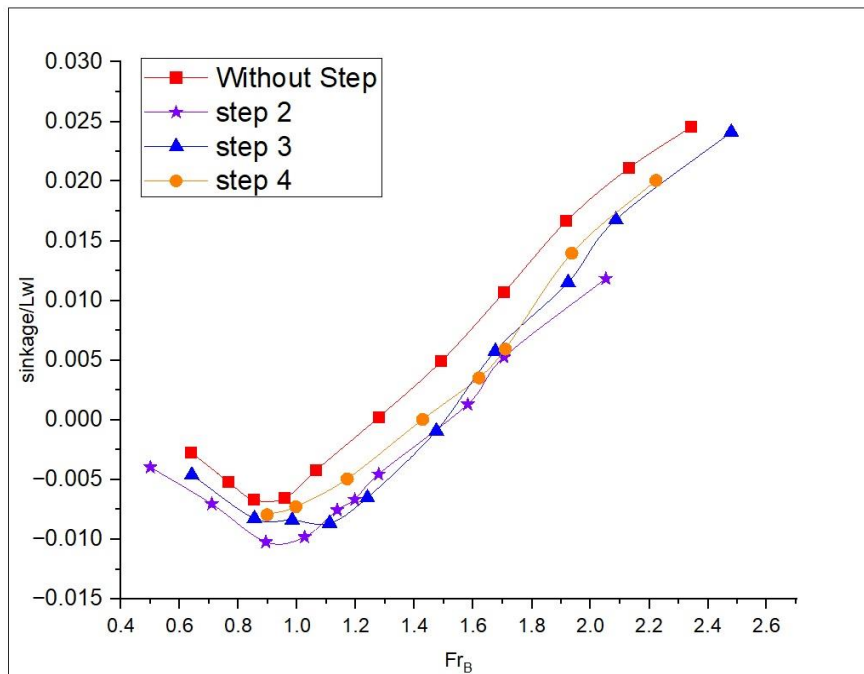


Fig. 19 Comparison of the sinkage/LWL values for different step locations and without step.

As seen in Fig. 18, steps are affecting the trim values by decreasing them. One transverse step application also effects the heave motion depicted in Fig. 19. The general trend of the curves with step applications is observed to be similar to the case without step application. In this case, the minimum s/LCB value, which is the step application located

close to the transom, prevents the hull from rising higher compared to other s/LCB locations. Controversially, it also means that the sinkage of the hull is slightly increasing when the step location is shifting in the $-x$ direction, especially after $Fr_B=1.50$.

In the Fig. 20, the variation of dimensionless overall resistance coefficient according to the beam Froude numbers by 4 different step locations and a bare hull without a step is depicted. Also, between $Fr_B = 0.75$ and 1.12, step 2 configuration leads to a slight decrease in the model's resistance. For, $Fr_B=1.12-1.68$, all step configurations have more resistance than the configuration without steps. As considering the boats with high speeds with steps, after $Fr_B=2.06$, configurations 2, 3 and 4 start to differentiate and reduce the resistance. In this special case, it's decided that the actual comparison should be in between the stepped cases in a range of Froude numbers ($Fr_B = 2.0-2.45$) for this type of hull.

Fig. 20 shows for step 1 and step 2 configurations up to $Fr_B = 1.1$, there is a slight reduction in resistance compared to the model without step. In between $Fr_B = 1.1$ and $Fr_B = 2.0$, all step configurations increase the resistance. Step 1 configuration, in the mentioned range of beam Froude numbers, increases the resistance more remarkably due to the pressure area in contact with the bottom of the hull close to the transom is very low (as refer to Fig. 16). Therefore, it has less lift affect on the body. Besides, effective resistance reduction starts about $Fr_B = 2.05$ for step 2-3 and step 4 configurations. In Fig. 21-a, the comparison of total displacement resistance coefficient of the model hull for different longitudinal step locations is given at certain beam Froude numbers.

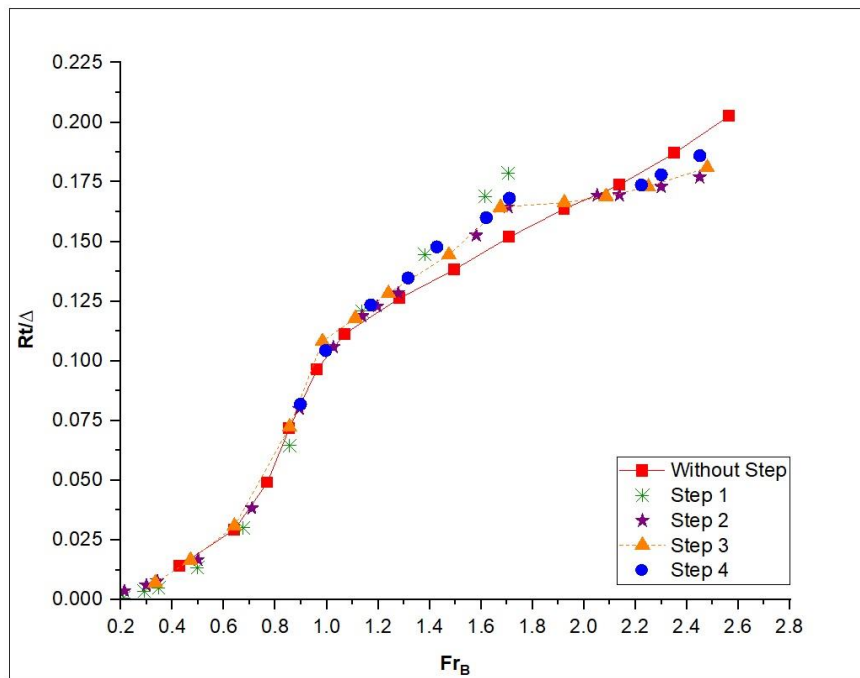


Fig. 20 Comparison of the $R_T(\Delta)$ of the hull without and with step of different step locations.

As seen in Fig. 21-a, at $Fr_B = 2.0$, the bare hull without a step configuration has the minimum resistance. $s/LCB=0.92$ gives minimum resistance and shifting the s/LCB to both backward ($-x$) and forward ($+x$), resistance starts to increase as compared to initial position. As seen in Fig. 21-a, at $Fr_B = 2.15$, the minimum resistance is at $s/LCB=0.86$ which is between step-2 and step-3 configurations. Shifting the s/LCB to both backwards ($-x$) and forward ($+x$) positions causes resistance to increase compared to the initial position.

As shown in Fig. 21-a, at $Fr_B=2.30$, the minimum resistance is obtained at $s/LCB= 0.75$. Additionally, $s/LCB=0.75$ which is close to the step-2 configuration is better than step-1 and

step-3 configurations. Also step-3 configuration is better than step-4 configuration while step-4 configuration is better than without step configuration.

From the curve corresponding to $Fr_B=2.45$, it is observed that the best location of s/LCB is 0.75 in the related case. The general comparison of the mentioned cases is illustrated in Fig. 21. As regarding the beam Froude numbers, the optimum step locations for minimum resistance values are given in Fig. 21-b. The optimum longitudinal location of the one transverse step for a similar relatively high-speed hull with the velocity up to $Fr_B = 2.50$ is assessed at $s/LCB= 0.74-0.75$ (with the mean value being 0.745) when considering the beam Froude numbers range between 2.30 and 2.45.

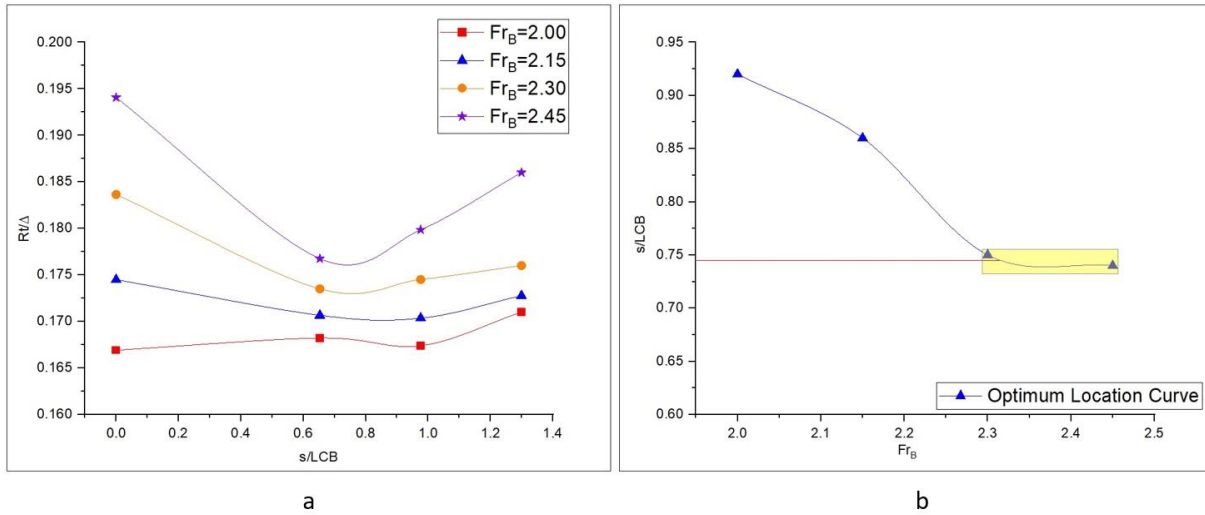


Fig. 21 a: s/LCB vs model total resistance over displacement ratio coefficients, **b:** Optimum one step longitudinal locations in respect to beam Froude numbers

6. Conclusions and future work

This research evaluates the optimum location of a single longitudinal transverse step through experiments for a relatively high-speed hull with the maximum velocity of approximately around $Fr_B = 2.50$. Before the experimental method of step applications, the original hull was tested to predict resistance characteristics as well as assessing trim and sinkage attitudes. To verify the experimental results, numerical methods were also used, and the results were compared to the full-scale trial data. RANS-based simulations were evaluated and compared to the model tests. It was determined that accurate prediction of the resistance of high speed boats can be achieved by eliminating the potential numerical ventilation problem. The following results were obtained from the high-speed model testing and numerical simulations:

- The numerical ventilation problem must be addressed for the numerical solutions for $Fr_B > 0.93$ by using phase change, and the estimated total resistance indicates quite reasonable consistency, with the experimental outcomes, with a margin of 2.86.
- Results in between $y^+ = 40$ and $y^+ = 60$ were consistent.
- The effective power requirement deviations according to the CFD analysis and experimental results were 1.7% and 1.6%, respectively.
- According to the study, by using numerical techniques with the help of aforementioned software, drag around a high-speed hull model can be efficiently utilized. The similar method might be used to simulate full-scale hull forms with more powerful computers.

- Trim values decrease in all cases after $Fr_B = 2.15$ and The rate of decrease in trim values is higher when s/LCB shifts in the $+x$ direction When step 4 is used, the minimum trim can be seen, whereas no step was used, the maximum trim value is observed.
- The application of steps is decreasing the unwanted trim values, which may also lead to a decrease in the overall resistance. Moreover, the rates of hull sinkage and rise also vary in relation to step positions due to the dynamic movements of the hull.
- In comparison to other s/LCB locations, the minimum s/LCB value that corresponds to step application is closest to the transom and prevents the hull from rising more.
- All step configurations have more resistance than those without steps when $Fr_B = 1.12-1.68$. For step 2-3 and step 4 configurations, effective resistance reduction commences at around $Fr_B = 2.05$. With this point of view, some phenomena can be noticed by viewing the wetted surfaces such as the spray pattern after the step and if the stagnation line crosses the step or not as stated in [38]. Concerning the importance of this aspect, [39] recommends that the wetted chine length should be at least 0.10 beams to avoid the origin of large, high-velocity spray sheets that can increase the total resistance and potentially cause longitudinal instability. The need to design a chine wetted forebody for stepped hulls is emphasized to avoid large increases in hydrodynamic resistance.
- The ideal longitudinal location of a single transverse step for a similar high-speed hull with a velocity of up to $Fr_B = 2.50$ was determined to be at $s/LCB=0.74-0.75$. This study focused on the beam Froude number range between 2.30 and 2.45, with a mean value of 0.745.

It was also found that the recommended numerical method can precisely predict high speed boat's resistance, trim, and sinkage. This study investigates on the optimum longitudinal location of one transverse step in calm water. The same procedure of this study is planned to be investigated in different wave conditions for a future plan.

ACKNOWLEDGMENTS

The authors would like to acknowledge the Ata Nutku Ship Model Basin staff at Istanbul Technical University for their assistance with the experiments. This study was partially funded by the ITU Scientific Research Projects Support Program under project ITU-BAP. The authors also appreciate Loça Mühendislik, the ship design company, for providing access to full-scale trial data.

REFERENCES

- [1] Samuel, S., Mursid, O., Yulianti, S., Kiryanto, K., Iqbal, M., 2022. Evaluation of interceptor design to reduce drag on planing hull. *Brodogradnja*, 73(3), 93-110. <https://doi.org/10.21278/brod73306>
- [2] Degiuli, N., Farkas, A., Martić, I., Zeman, I., Ruggiero, V., Vasiljević, V., 2021. Numerical and experimental assessment of the total resistance of a yacht. *Brodogradnja*, 72(3), 61-80. <https://doi.org/10.21278/brod72305>
- [3] Svahn, D., 2009. Performance prediction of hulls with transverse steps (M. Sc. thesis). *KTH Centre for Naval Architecture*, Stockholm, Sweden.
- [4] Garland, W. R., Maki, K. J., 2012. A numerical study of a two-dimensional stepped planing surface. *Journal of Ship Production and Design*, 28(02), 60-72. <https://doi.org/10.5957/jspd.2012.28.2.60>
- [5] Lee, E. J., 2014. Advancements of stepped planing hulls (Doctoral dissertation), *Virginia Tech*, Blacksburg, VA.
- [6] Lotfi, P., Ashrafizaadeh, M., Esfahan, R. K., 2015. Numerical investigation of a stepped planing hull in calm water. *Ocean engineering*, 94, 103-110. <https://doi.org/10.1016/j.oceaneng.2014.11.022>
- [7] Malek, A., Koto, J., 2017. Study on Resistance of Stepped Hull Fitted with Interceptor Plate. *Science and Engineering*, 39, 18-22.

- [8] De Marco, A., Mancini, S., Miranda, S., Scognamiglio, R., Vitiello, L., 2017. Experimental and numerical hydrodynamic analysis of a stepped planing hull. *Applied Ocean Research*, 64, 135-154. <https://doi.org/10.1016/j.apor.2017.02.004>
- [9] Ghadimi, P., Panahi, S., 2019. Numerical investigation of hydrodynamic forces acting on the non-stepped and double-stepped planing hulls during yawed steady motion. *Proceedings of the Institution of Mechanical Engineers, Part M: Journal of Engineering for the Maritime Environment*, 233(2), 428-442. <https://doi.org/10.1177/1475090217751549>
- [10] Kazemi, H., Salari, M., Nowruzi, H., Najafi, A., 2019. Hydrodynamics analysis of stepped planing hull under different physical and geometrical conditions. *Journal of the Brazilian Society of Mechanical Sciences and Engineering*, 41(9), 1-12. <https://doi.org/10.1007/s40430-019-1866-9>
- [11] Bilandi, R. N., Vitiello, L., Mancini, S., Nappo, V., Roshan, F., Tavakoli, S., Dashtimanesh, A., 2020. Calm-water performance of a boat with two swept steps at high-speeds: Laboratory measurements and mathematical modeling. *Procedia Manufacturing*, 42, 467-474. <https://doi.org/10.1016/j.promfg.2020.02.046>
- [12] Esfandiari, A., Tavakoli, S., Dashtimanesh, A., 2020. Comparison between the dynamic behavior of the non-stepped and double-stepped planing hulls in rough water: a numerical study. *Journal of Ship Production and Design*, 36(01), 52-66. <https://doi.org/10.5957/jspd.2020.36.1.52>
- [13] Najafi, A., Nowruzi, H., Ameri, M. J., 2020. Hydrodynamic assessment of stepped planing hulls using experiments. *Ocean Engineering*, 217, 107939. <https://doi.org/10.1016/j.oceaneng.2020.107939>
- [14] Samedi, S. M., Ghadimi, P., 2020. Experimental and numerical investigation of stepped planing hulls in finding an optimized step location and analysis of its porpoising phenomenon. *Mathematical Problems in Engineering*, 2020, 3580491. <https://doi.org/10.1155/2020/3580491>
- [15] Bilandi, R. N., Tavakoli, S., Dashtimanesh, A., 2021. Seakeeping of double-stepped planing hulls. *Ocean Engineering*, 236, 109475. <https://doi.org/10.1016/j.oceaneng.2021.109475>
- [16] Husser, N., Brizzolara, S., 2021. The Impact of Sweep Angle on Stepped Planing Hull Performance. *SNAME International Conference on Fast Sea Transportation*, October 26–27, Providence, Rhode Island, USA. <https://doi.org/10.5957/FAST-2021-010>
- [17] Ghadimi, P., Sajedi, S. M., Ghadimi, A., Sheikholeslami, M., 2022. Experimental and numerical investigation of the effects of incorporation of one and two steps to a mono-hull planing vessel on its performance in calm water. *Scientia Iranica*, 29(3), 1169-1184.
- [18] Nowruzi, H., 2022. Performance prediction of stepped planing hulls using experiment and ANNs. *Ocean Engineering*, 246, 110660. <https://doi.org/10.1016/j.oceaneng.2022.110660>
- [19] Yang, D., Sun, Z., Jiang, Y., Gao, Z., 2019. A study on the air cavity under a stepped planing hull. *Journal of Marine Science and Engineering*, 7(12), 468. <https://doi.org/10.3390/jmse7120468>
- [20] Najafi, A., Nowruzi, H., Ameri, M. J., Karami, M., 2021. An experimental study of the wetted surfaces of two-stepped planing hulls. *Ocean Engineering*, 222, 108589. <https://doi.org/10.1016/j.oceaneng.2021.108589>
- [21] Vitiello, L., Mancini, S., Bilandi, R. N., Dashtimanesh, A., De Luca, F., Nappo, V., 2022. A comprehensive stepped planing hull systematic series: Part 1-Resistance test. *Ocean Engineering*, 266, 112242. <https://doi.org/10.1016/j.oceaneng.2022.112242>
- [22] Panahani, R., Jahanbakhsh, E., Seif, M. S., 2009. Towards simulation of 3D nonlinear high-speed vessels motion. *Ocean Engineering*, 36, 256-265. <https://doi.org/10.1016/j.oceaneng.2008.11.005>
- [23] Dogrul, A., 2022. Numerical prediction of scale effects on the propulsion performance of Joubert BB2 submarine. *Brodogradnja*, 73(2), 17-42. <http://doi.org/10.21278/brod73202>
- [24] Patankar, S. V. and Spalding, D.B., 2005. A calculation procedure for heat, mass and momentum transfer in three-dimensional parabolic flows. *International Journal of Heat and Mass Transfer*, 15(2), 1787-1806. [https://doi.org/10.1016/0017-9310\(72\)90054-3](https://doi.org/10.1016/0017-9310(72)90054-3)
- [25] Avci, A. G., Barlas, B., 2018. An experimental and numerical study of a high-speed planing craft with full-scale validation. *Journal of Marine Science and Technology*, 26(5), 617-628. [https://doi.org/10.6119/JMST.201810_26\(5\).0001](https://doi.org/10.6119/JMST.201810_26(5).0001)
- [26] Dixit, S.A., Ramesh, O.N., 2009. Determination of skin friction in strong pressure-gradient equilibrium and near equilibrium turbulent boundary layers. *Experiments in Fluids*, 47(6), 1045-1058. <https://doi.org/10.1007/s00348-009-0698-2>
- [27] CD-Adapco., 2014. *User guide STAR-CCM+ Version 9.0.2*.

- [28] Tezdogan, T., Demirel, Y.K., Kellett, P., Khorasanchi, M., Incecik, A., Turan, O., 2015. Full-scale unsteady rans CFD simulations of ship behaviour and performance in head seas due to slow steaming. *Ocean Engineering*, 97,186-206. <https://doi.org/10.1016/j.oceaneng.2015.01.011>
- [29] ITTC., 2008. Testing and Extrapolation Methods High Speed Marine Vehicles, *Specialist Committee on Powering Performance Prediction 25th ITTC*. Available from: <https://itcc.info/media/1279/75-02-05-01.pdf> (accessed 15.11.22).
- [30] Federici, A., 2014. Design and analysis of nonconventional hybrid high-speed hulls with hydrofoils by CFD methods. *University of Genoa*, Genoa, Italy.
- [31] Lee, E., Pavkov, M., McCue-Weil, L., 2014. The systematic variation of step configuration and displacement for a double-step planing craft. *Journal of Ship Production and Design*, 30(02), 89-97. <https://doi.org/10.5957/jspd.2014.30.2.89>
- [32] Avci, A.G., 2022. A parametric investigation of hydrodynamic performance for a high-speed hull in cases with interceptor and step (Ph.D. dissertation). *Istanbul Technical University*, Istanbul, Turkey.
- [33] Delen, C., Bal, Ş., 2015. Uncertainty analysis of resistance tests in Ata Nutku Ship Model Testing Laboratory of Istanbul Technical University. *Journal of Maritime and Marine Sciences*, 1(2), 8-27.
- [34] Roache, P. J., 1998. Verification and validation in computational science and engineering (Vol. 895, p. 895). *Albuquerque*, NM: Hermosa.
- [35] Celik, I.B.; Ghia, U.; Roache, P.J.; Freitas, C.J., 2008. Procedure for Estimation and Reporting of Uncertainty Due to Discretization in CFD Applications. *ASME: The Journal of Fluids Engineering*, 130, 078001. <https://doi.org/10.1115/1.2960953>
- [36] Castaldi, L., Osmak, F., Green, M., Fürth, M., & Bonoli, J., 2021. The effect of spray deflection on the performance of high speed craft in calm water. *Ocean Engineering*, 229, 108892. <https://doi.org/10.1016/j.oceaneng.2021.108892>
- [37] Eça, L., Hoekstra, M., 2006. Discretization uncertainty estimation based on a least squares version of the grid convergence index. In *Proceedings of the Second Workshop on CFD Uncertainty Analysis*, Lisbon, Portugal, Instituto Superior Técnico, 1-27.
- [38] Eça, L., Hoekstra, M., 2014. A procedure for the estimation of the numerical uncertainty of CFD calculations based on grid refinement studies. *Journal of computational physics*, 262, 104-130. <https://doi.org/10.1016/j.jcp.2014.01.006>
- [39] Savitsky, D., Morabito, M., 2010. Surface wave contours associated with the forebody wake of stepped planing hulls. *Marine Technology SNAME*, 47(01), 1-16. <https://doi.org/10.5957/mtsn.2010.47.1.1>

Submitted: 17.11.2022

Ahmet Gultekin Avci*, agavci@yildiz.edu.tr

*Corresponding author

Accepted: 07.05.2023.

Yildiz Technical University, Faculty of Naval Architecture and Maritime,
34349 Besiktas, Istanbul, Turkey.

Baris Barlas, barlas@itu.edu.tr

Istanbul Technical University, Faculty of Naval Architecture and Ocean
Engineering, 34469 Maslak, Istanbul, Turkey.